E.S. Dehghani, S. Aghion, W. Anwand, G. Consolati, R. Ferragut, G. Panzarasa
Investigating the Structure of Crosslinked Polymer Brushes (Brush-Gels) by means of Positron Annihilation Spectroscopy
European Polymer Journal, Vol. 99, 2018, p. 415-421
doi:10.1016/j.eurpolymj.2017.12.042

Investigating the structure of crosslinked polymer brushes (brush-gels) by means of Positron Annihilation Spectroscopy

Ella S. Dehghani[1], Stefano Aghion[2,3], Wolfgand Anwand[4], Giovanni Consolati[5,3], Rafael Ferragut[2,3], Guido Panzarasa[6]

[1] Laboratory of Surface Science and Technology (LSST), Department of Materials, ETH, Vladimir-Prelog-Weg 5, 8093 Zürich, Switzerland.

[2] LNESS, Department of Physics, Politecnico di Milano, via Anzani 42, 22100 Como, Italy.

[3] INFN, Sezione di Milano, via Celoria 16, 20133 Milano, Italy.

[4] Institute of Radiation Physics, Helmholtz-Zentrum Dresden-Rossendorf, Bautzner Landstr. 400,01328 Dresden, Germany.

[5] Department of Aerospace Science and Technology, Politecnico di Milano, via La Masa 34, 20156 Milano, Italy.

[6] Empa Materials Science and Technology, Laboratory for Biomimetic Membranes and Textiles, Lerchenfeldstrasse 5, 9014 St. Gallen, Switzerland.

Abstract

Polymer brushes can be useful as small-scale reactors for the controlled synthesis of nanoparticles, an approach which is gaining increasing interest. In this context, chemical crosslinking of polymer brushes could be considered as a viable approach to control the size and size distribution of the formed nanoparticles. Here we describe the application of Positron Annihilation Spectroscopy (PAS) for the characterization of crosslinked polymer brushes (brush-gels). Poly(hydroxyethyl methacrylate) (PHEMA) brushes were obtained on silicon substrates by means of a surface-initiated atom transfer radical polymerization (SI-ATRP). Crosslinking was achieved during the polymerization by adding different amounts of diethyleneglycol dimethacrylate (DEGDMA) as a difunctional monomer. The resulting brushes, both un- and crosslinked, were then post-modified with carboxylic acid groups, allowing the *in situ* synthesis of silver nanoparticles after ion exchange with silver nitrate and reduction with sodium borohydride. The detailed characterization of such systems is notoriously challenging and PAS proved to be an effective, non-invasive technique to acquire insight on the structure of the brushes and of their nanoparticle composites.

1. Introduction

Polymer brushes are dense assemblies of polymer chains tethered by one end to a surface [1], [2]. Thanks to the proximity of neighboring chains, such configuration gives rise to distinctive properties. Applications for such systems are widespread and range, to name a few, from smart surfaces to sensors and actuators [3], microfluidics [4], tribology [5], drug delivery [6], [7] and organic electronics [8]. If chemical bonds are introduced between the polymer chains, that is, if the brushes are crosslinked, then the so-called "brush-gel" can be obtained. Crosslinking can be achieved either via post-functionalization reactions [9], [10] or during the polymerization process itself, by introducing a bifunctional monomer [11]. The resulting brush-gels combine the properties of polymer brushes and of hydrogels, making them versatile nanoreactors [12]. Brush-gels can be used as matrixes for the controlled synthesis of nanoparticles, with the possibility to tune

the size of the latter as a function of the macromolecular structure (e.g. degree of crosslinking) of the brush template. Moreover, the crosslinked scaffold provides additional stability to the particles, reducing the risk of leaching and improving the overall performance of the device [13]. The introduction of plasmonic (noble metal), magnetic (magnetite) or semiconducting (quantum dots) nanoparticles into robust, responsive polymer layers, opens new pathways for the engineering of composite nanostructured films exhibiting mechanical, electrical, magnetic and optical properties, with the potential to be used for the development of functional platforms [14].

The characterization of polymer brushes, especially when decorated with nanoparticles, is a challenging task requiring the combination of many different techniques. The thickness of polymer brushes is usually determined by means of spectroscopic ellipsometry or X-ray reflectivity, while Fourier-transform infrared spectroscopy (FT-IR) and X-ray photoelectron spectroscopy (XPS) can provide information on the chemical constitution. Morphological analysis can be obtained by means of scanning probe microscopy or electron microscopy, but, if the brushes contain nanoparticles, then it is usually necessary to perform electron microscopy on cut sections (i.e. to destroy the sample) to analyze the particles' spatial distribution. Our group has already demonstrated how the application of positron annihilation spectroscopy (PAS), a non-destructive technique able to probe nanometer-scale vacancies and defects, opens up a completely new perspective to look at polymer brushes. In our previous works [15], [16] we studied the physico-chemical changes associated with protonation and embedding of silver nanoparticles in brushes made of poly(dimethylaminoethyl methacrylate) (PDMAEMA), a well-known pH-responsive polymer. Here, we complement and extend our work by studying carboxylic acid-modified poly(hydroxyethyl methacrylate) (PHEMA) brush-gels. Using PAS, within a single analysis it was possible to determine the changes associated with different degrees of crosslinking and the incorporation of silver nanoparticles, which is otherwise difficult to obtain with more conventional techniques.

2. Materials

10-Undecen-1-ol, 2-bromoisobutyryl bromide, dimethylchlorosilane, succinic anhydride, pyridine, 2,2'-bipyridyl, copper(I) chloride, copper(II) bromide, sodium borohydride, silver nitrate, hydrochloric acid, sulfuric acid and hydrogen peroxide (35%) were purchased from Aldrich-Fine Chemicals Switzerland, and used as received. Anhydrous tetrahydrofuran (99.5%, extra dry) was purchased from Acros Germany. Hydroxyethyl methacrylate (HEMA) (Aldrich-Fine Chemicals, Switzerland) was purified according to a procedure described by Baker et al. [17] Diethyleneglycol dimethacrylate (DEGDMA) (Aldrich-Fine Chemicals, Switzerland) was passed through a column of basic alumina prior to use. Water was deionized with a GenPure filtration system (18.2 MΩ cm, TKA, Switzerland).

2.1. Surface-initiated atom-transfer radical polymerization (SI-ATRP) and incorporation of silver nanoparticles

The synthesis of the silane-based initiator 11-(2-bromo-2-methyl-propionyl)-dimethylchlorosilane (BPCS) for SI-ATRP was carried out in accordance with the already reported protocol by Sanjuan et al. [11], [18]. Self-assembled monolayers (SAMs) of BPCS on silicon oxide substrates were obtained by wet deposition. Namely, silicon substrates were first cleaned by immersion in piranha solution (70 vol% of sulfuric acid and 30 vol% of hydrogen peroxide) (warning: piranha solution is very reactive and corrosive; use extreme caution!) followed by extensive rinsing with water and drying with a nitrogen stream. Subsequently, the substrates were immersed overnight in a 10 mM BPCS solution in dry toluene, rinsed with toluene and dried with a nitrogen stream.

PHEMA brushes and brush-gels were grown from BCPS SAMs using SI-ATRP of different HEMA/DEGDMA mixtures, applying a catalytic system comprising CuCl (55 mg, 0.55 mmol), $CuBr_2$ (36 mg, 0.16 mmol), and 2,2'-bipyridyl (244 mg, 1.56 mmol) in a 1:1 mixture of monomer and water (4:4 mL) [11]. The mixture of

solvent, monomer and ligand was bubbled with nitrogen for half an hour to remove dissolved oxygen, after which the solution was transferred to a flask containing the CuCl and $CuBr_2$ kept under nitrogen. The resulting solution was stirred for 30 min following the complete formation of the catalyst complex (dark-brown solution). The polymerization solution was then transferred to the flask containing the BPCS-functionalized silicon oxide substrates, and the reaction proceeded for 1 h.

Following the polymerization, the samples were removed from the solution and rinsed extensively with ethanol and water. To introduce carboxylic acid functions on the PHEMA chains, the modified wafers were immersed overnight in a 0.5 M succinic anhydride solution in dry pyridine, rinsing with dry pyridine afterwards and drying.

Subsequent overnight incubation of the substrates in a 0.05 M solution of silver nitrate in water, overnight, led to the formation of the carboxylate–silver complex. Then, the substrates were treated with a 1 µM solution of sodium borohydride ($NaBH_4$) in water for 10 s to allow formation of silver nanoparticles (AgNPs). The substrates were then rinsed with MilliQ water and dried with a nitrogen stream.

2.2. Characterization

The dry thickness of brushes and brush-gels was measured with a variable-angle spectroscopic ellipsometer (VASE) (M-2000F, LOT Oriel GmbH, Darmstadt, Germany). The samples were analyzed before the incorporation of AgNPs. The measurements were carried out under the assumption that the dry polymer film has a refractive index of 1.45, and applying a three-layer model (SiO_2/Cauchy (initiator)/Cauchy (PHEMA)) with SiO_2 and initiator layers having fixed thicknesses and refractive indices (software WVASE32, LOT Oriel GmbH, Darmstadt, Germany). A Cauchy model, $n = A + B/\lambda^2$, was used to describe the refractive index of the PHEMA films by means of two fitting parameters: offset (A = 1.45) and wavelength dispersion (B = 0.01). To measure the swelling ratio, ellipsometry was performed in MilliQ water using a custom-built liquid cell and applying a four-layer model (SiO_2/Cauchy (initiator)/Cauchy (PHEMA)/ambient (water)), with the refractive index of water set at 1.33. The swollen thickness was analyzed with an effective-medium approximation (EMA) model, featuring both Cauchy and water components.

FT-IR spectra were recorded in transmission mode on dried samples by employing an infrared spectrometer (Bruker, IFS 66 V) equipped with a liquid-nitrogen-cooled MCT detector. A background spectrum was collected from a freshly cleaned silicon wafer. The chemical composition of brushes and brush-hydrogels was analyzed by X-ray photoelectron spectroscopy (XPS). XPS measurements were performed using a Theta-Probe X-ray photoelectron spectrometer (ARXPS, Thermo Fisher Scientific, Waltham MA, USA), with a monochromatic Al K α source with a beam diameter of 300 µm. High-resolution spectra of carbon and oxygen with a pass energy of 100 eV were collected. Three measurements were performed for each sample, all containing the survey spectra. The system was equipped with a combined low-energy electron/ion flood gun for charge compensation. The measurements were performed in standard lens mode with an emission angle of 53° to the surface and an acceptance angle of ±30°. Non-destructive elemental depth analysis was done using angle-resolved X-ray photoelectron spectroscopy (ARXPS). Angle-resolved XPS analysis was performed by allowing the instrument to the parallel acquisition of angle-resolved spectra, without tilting the sample, to collect the data at different emission angles simultaneously. The ARXPS measurements were performed with a Theta-Probe X–ray photoelectron spectrometer (ARXPS, Thermo Fisher Scientific, Waltham MA, USA), equipped with a monochromatic Al Kα source and a beam diameter of 300 µm. The pass energy was 100 eV for the high-resolution spectra of carbon, oxygen and nitrogen elemental analysis, while the pass energy of the survey spectrum was 200 eV. To compensate for the charging occurring at the surface, an electron-argon-ion flood gun was used. Three measurements were performed for each sample in the 8 different emission angles to the surface, ranging from 26.7° to 79.2°.

A LEO Gemini scanning electron microscope from Carl Zeiss (Germany) with a Schottky-field emission cathode was used to conduct the SEM investigations. All images were converted to 8-bit-grey-scale images

for image processing. To increase conductivity and avoid accumulation of electrostatic charges, the samples were sputter-coated with 1.3 nm of platinum using a Cressington HR208 sputter-coater and a Cressington mtm20 thickness controller. Visualization of samples' topography was performed by an in-lens and a secondary electron detector at an acceleration voltage of 3 kV. To investigate the surface roughness and topography of polymer brushes and brush-gels, a Bruker Dimension Icon® atomic force microscope (AFM) was used in tapping and peak force mode. The cantilever resonance and the spring constant was 300 kHz and 40 N m^{-1}, respectively.

PAS measurements were conducted by means of a positron beam at the HZDR in Dresden (Germany). [19] Forty values for the positron implantation energy were chosen between 0.03 keV and 32 keV and, for each energy value, a hyperpure Ge detector coupled with a MCA system recorded the annihilation spectrum. The positron annihilation peak is centered at 511 keV. Its broadening is a consequence of the Doppler effect due to the electron-positron center of mass momentum respect to the laboratory frame of reference. The *S*-parameter is then defined as the ratio between the area in the central part of the annihilation peak, within the energy range of 511 ± 0.85 keV ($|p_L| \leq 0.456$ atomic units). The *W*-parameter ("wing" or core annihilation parameter) is taken in the high-momentum region far from the center part of the peak, within the range from 511 ± 1.8 keV to 511 ± 4 keV. The total area of the peak is taken in the range 511 ± 4.25 keV.

For each implantation energy, the *S*-parameter and the three-gamma fraction $F_{3\gamma}$ were measured and are showed in Fig. A5. The *S*-parameter corresponds to the annihilation of the positrons with the valence electrons of the material, p-Ps annihilation or the o-Ps atoms undergoing a pick-off annihilation. The three-gamma fraction $F_{3\gamma}$ is calculated according to the "*3γ* method". When the studied material contains big cavities (>1 nm), the annihilation of o-Ps in three gamma-rays is observed and in this case $F_{3\gamma}$ is proportional to the Ps yield. The energy distribution of each of the three gamma rays is continuous between 0 and 511 keV. By defining *R(E), E* being the positron implantation energy, as:

$$R(E) = \frac{V}{P} \tag{1}$$

where *P* are the integrated counts in the peak area, within the energy region 511 ± 4.25 keV, and *V* is the valley area above the Compton edge, from 350 keV up to 500 keV, the three-gamma fraction $F_{3\gamma}$ is given by:

$$F_{3\gamma} = \left[1 + \frac{P_1}{P_0}\frac{R_1 - R(E)}{R(E) - R_0}\right]^{-1} \tag{2}$$

where the subscripts 0 and 1 refer to the cases with 0% and 100% Ps production, respectively [20].

3. Results and discussion

3.1. Brushes and brush-gels obtained by SI-ATRP and successive incorporation of silver nanoparticles

PHEMA-based brushes and brush-gels were synthesized by SI-ATRP from initiator-functionalized silicon oxide substrates. The use of an aqueous solvent during the polymerization allowed the grafting of around 100 nm-thick films in a relatively short time (1 h). This was due to the well-known accelerating effect of water, which increased the relative concentration of propagating macro-radicals due to the stabilization of Cu(I)complex species [17]. As downside, such a rapid growth can occur at the expense of the overall polymerization control, leading e.g. to a reduced chain re-initiation efficiency due to the loss of terminal initiator groups. However, for the purposes of our study, these issues can be neglected. PHEMA-based

brush-gels were synthesized using DEGDMA as crosslinker, which was introduced in the SI-ATRP feed with a 2 mol% and 4 mol% relative concentration compared to HEMA (See Fig. 1).

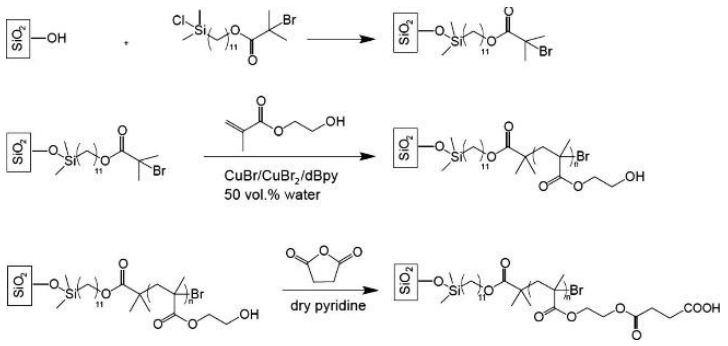

Fig. 1. Schematic representation of the procedure used to obtain PHEMA brushes and PHEMA-SA brushes.

For the sake of clarity, brushes and brush-gels obtained with different crosslinker contents will be named PHEMA for the brushes, while PHEMA-DEG-2 and PHEMA-DEG-4 will indicate brush-gels synthesized with 2 mol% and 4 mol% DEGDMA, respectively. Their composition was investigated by FT-IR and no significant difference was observed between the spectra of brushes and of brush-gels (Fig. A1a). In all spectra, the strong peak at 1750 cm^{-1} is related to $C{=}{=}O$ stretching, while the alkane stretching vibration and broad alcohol stretch peaks are recognizable at 2800–3000 and 3500 cm^{-1}, respectively. The quantitative analysis of crosslinker concentration in the polymer network was studied by XPS (Table A1). The elemental composition from the survey spectrum (69.9% carbon and 30.1% oxygen) was within the error of the expected composition for the PHEMA film (66.7% carbon and 33.3% oxygen, 4% error).

The C1s peak for PHEMA was resolved into five component peaks: a hydrocarbon ($C-C$) peak at 285 eV, a quaternary carbon (q-C) peak at 285.6 eV, a hydroxyl ($C-OH$) peak at 286.4 eV, an ether ($C-O$) peak at 287 eV, and a carbonyl ($O-C{=}{=}O$) peak at 289.1 eV (Fig. A2a). The binding energies and the relative areas of all these peaks were consistent with the structure of PHEMA, as previously reported [21]. In order to quantify the crosslinker concentration in the brush-hydrogel films, the C1s peak recorded for brush-gels was also resolved with the same component peaks. To estimate the crosslinker concentration, we employed equation 1, where A is the calculated area of the Csingle bondOH peak from XPS C1s (summarized in Table A1) [11], [21].(3)

$$\textit{Mol\% of Crosslinker} = (A_{brush} - A_{brush\ hydrogel})/A_{brush} \quad (3)$$

By increasing the amount of crosslinker in the polymerization feed from 2 mol% to 4 mol%, the effective concentration of DEGDMA within each brush-gel sample was found to be 11 ± 3 mol% and 20 ± 3 mol%, respectively. Both brushes and brush-gels were subsequently reacted with succinic anhydride (SA) to functionalize the hydroxyl side chains of the PHEMA backbones with carboxylic acid groups. Following the reaction with SA, the FT-IR absorbance profiles showed the appearance of a clear signal at 1500–1700 cm^{-1} related to the carboxylate stretching. In addition, the broad band between 3000 cm and 1 and 3700 cm^{-1} related to the –OH stretching peak disappeared, confirming the nearly quantitative derivatization of the hydroxyl groups (Fig. A1b). The C1s peaks obtained by XPS were resolved into five component peaks, originating from the functional groups within the monomer units and the succinic anhydride (Fig. A2b). After modification with succinic anhydride, from the elemental analysis of carbon and oxygen, the concentration of carboxylic groups was measured to be >90% [22].

The introduction of succinate moieties along the brush backbones induced an increase of thickness in all the films studied. PHEMA brushes increased their average thickness by 188%, reaching 288 ± 5 nm, after SA functionalization (sample PHEMA-SA). In a similar way, brush-gels showed a relevant increase in dry thickness, of 127% and 100% for PHEMA-DEG-2-SA and PHEMA-DEG-4-SA, respectively [11], [23]. Subsequent overnight incubation of the substrates in a 0.05 M aqueous solution of silver nitrate led to the

formation of the carboxylate–silver complexes. Then, the samples were treated with a 1 µM solution of sodium borohydride in water for 10 s to allow the formation of silver nanoparticles (AgNPs) [12]. Each step was characterized by atomic force microscopy (AFM), ellipsometry, and XPS. From AFM analysis, the average size and the size distribution of the nanoparticles could be determined. Average diameters of 33 ± 14 nm, 23 ± 8 nm and 12 ± 5 nm were found for the AgNPs generated respectively in PHEMA-SA brushes, PHEMA-DEG2-SA and PHEMA-DEG4-SA brush-gels. From the experimental results, it can be deduced that by increasing the amount of crosslinker, smaller particles were formed within the polymer films (Fig. 2; see also Fig. A3).

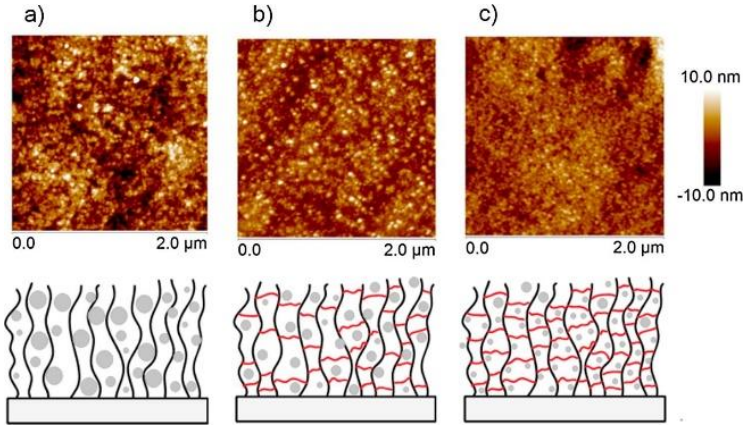

Fig. 2. AFM images (tapping mode) and schematic representations of the brushes and brush-gels after in situ formation of silver nanoparticles: (a) PHEMA-SA-Ag; (b) PHEMA-DEG2-SA-Ag; (c) PHEMA-DEG4-SA-Ag. The samples were analyzed in the dry state. The polymer chains are in black, the crosslinker units are represented in red and AgNPs as grey circles.

XPS measurements showed that at higher emission angles, i.e. for surface-sensitive measurements, the ratio of carbon to silver peak decreased for all brushes. Interestingly, PHEMA-DEG2-SA hybrids with silver nanoparticles showed the highest carbon-to-silver ratio for all emission angles (Fig. A4). The carbon/silver ratio at different emission angles was also measured for the samples after incubation in silver nitrate and treatment with sodium borohydride (Table A2). However, both AFM and XPS are sensitive only to the very surface layer, maximum 10 nm inside, while our samples are hundreds of nanometers (100–300 nm) thick. The SEM of a representative fractured sample demonstrates that the silver nanoparticles are homogeneously distributed inside the polymer layer (Fig. A5). The nanoparticles did not show any tendency to aggregate or detach following immersion in water. This is presumably due to the coordination stabilization by the oxygen atoms present both on DEGDMA and on HEMA, and by steric stabilization which is gained by embedment in the brush structure [12].

3.2. Positron annihilation spectroscopy

The profiling of brushes as a function of the crosslinker content and of the presence of AgNPs was studied by means of positron annihilation spectroscopy, taking advantage of the Doppler broadening technique. Fig. 3 shows the *S*-parameter evolution of the brushes as a function of the positron implantation energy. For all samples, the curves were found to converge in the same zone at high energies, meaning that the positrons have reached the underlying silicon substrate. However, there is a clear difference in the behavior of the *S*-parameter between the samples before and after the formation of silver nanoparticles (AgNPs), while the influence of the DEGDMA crosslinker appears to be less important in samples without AgNPs.

The positrons implanted into the brushes mainly annihilate inside the molecular microstructure of the polymer, in sub-nanometric free volumes within polymer chains and nanometric cavities between brushes. Positronium atoms (Ps) are formed inside free volumes and cavities. Among the samples without AgNPs, the evolution of the PHEMA-DEG-2-SA sample (full red symbols) is characterized by higher brush-zone *S*-parameter values. Since the chemical environment where the positrons annihilate is expected to be the

same as for sample PHEMA-DEG-4-SA, that difference is attributed to a higher efficiency of Ps formation. Fig. A6 shows that the distribution of Ps three-gamma fraction $F_{3\gamma}$ in the sample PHEMA-DEG-2-SA is over the other two distributions. This indicates that this sample contains more open volumes (with a size of the order or higher than 1 nm), where *ortho*-Ps is formed [15], [24]. Presumably, in this sample, the chains are more separated and thus the brushes more disordered.

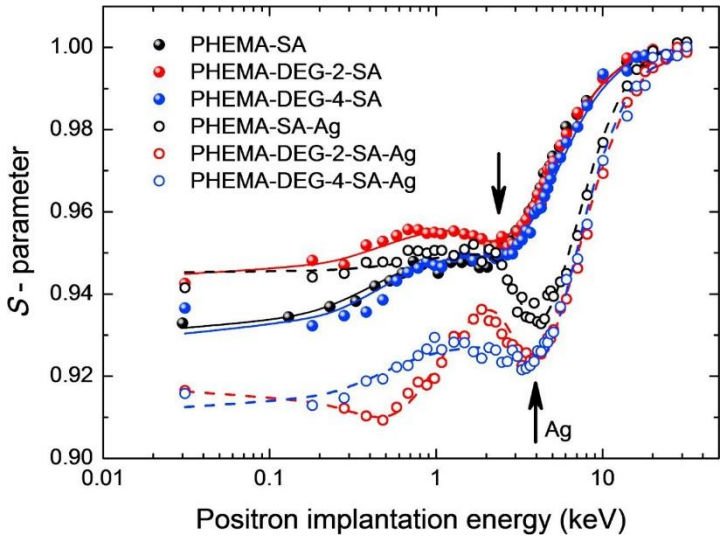

Fig. 3. Normalized *S*-parameter as a function of the positron mean implantation energy for various samples of PHEMA-based brushes on silicon substrates: full symbols represent as-made samples with 0, 2 and 4% of DEGDMA as crosslinker, and open symbols represent the samples after AgNPs formation (Ag). The lines through the experimental data represent the results of a best-fit procedure obtained with VEPFIT. The *S*-parameter was normalized to the Si substrate value. The upper and lower arrows indicate the implantation energy whose mean implantation depth corresponds to the average thicknesses of the brushes before and after silver formation, respectively. The error bar is within the symbols of the experimental points.

As can be observed in Fig. 3, after the formation of AgNPs (samples "-Ag", open symbols), the *S*-parameter distributions are shifted towards higher implantation energies. The arrows in Fig. 3 indicate that the implantation energy, whose mean implantation depth corresponds to the average thicknesses of the brushes, is higher after AgNPs formation. The above-mentioned shift is symptomatic of an increase of the overall density of the brush-nanoparticle systems [15].

In the samples loaded with AgNPs (identified in Fig. 3 with the suffix "Ag") a fraction of the positrons is implanted both in the polymer and into the metallic particles. The latter fraction is nearly proportional to the volume fraction of the nanoparticles, which is between 13 and 19% (as it will be discussed later). Since the positron diffusion length in Ag is considerably higher than the average NPs size, the probability of annihilation inside their bulk is low. Indeed, the positron diffusion length in silver with a low density of defects is typically between 50 and 100 nm [25], [26] but the average diameter of the nanoparticles is between 12 and 33 nm. According to our estimation, only a fraction between 0.4 and 4% of the total implanted positrons annihilates into the nanoparticles, and between 3 and 20% of the positrons implanted into the AgNPs (see eq. A1, originally proposed for nanograins) [27]. The majority of the positrons implanted into the AgNPs migrate and annihilate at the nanoparticles' surface. In appendix A, a representation of the *W*-parameter as a function of the *S*-parameter is also available (Fig. A7), which additionally demonstrates the influence of the presence of silver on PAS results. The comparison between the *W*-*S* distribution in samples without and with AgNPs presented in Fig. A7 shows that the samples that contain silver tend slightly to the Ag "pole" represented by the measure of a nearly pure (99.999%) bulk silver sample.

The main difference between the samples with and without Ag is the drop at the brush/substrate interface zone when AgNPs are present (Fig. 3, shown by an arrow). This drop is attributed to residual sub-nanometric metallic particles and/or to trapped molecules (such as BH_4^-, BO_3^{3-}, NO_3^-) that sit at the interface. In this context, after the formation of AgNPs, the brushes at the interface zone remain charged

with the residual particles/molecules that inhibit and quench positronium, with the decrease of the *S*-parameter as a net effect. It should be emphasized that the presence of both crosslinker and silver nanoparticles lowers the *S*-parameter value in correspondence of the brushes region, especially for the samples PHEMA-DEG-2-SA-Ag and PHEMA-DEG-4-SA-Ag. In these latter samples, two competitive phenomena can occur: (i) Ps inhibition by the influence of residual impurities; and (ii) positron annihilation in a silver environment (mainly at the nanoparticles' surface). On the other hand, the formation of AgNPs in the sample without crosslinker (PHEMA-SA-Ag), apparently does not affect the *S*-parameter in the brushes zone. Moreover, its *S*-parameter at the surface is similar to the value of sample PHEMA-DEG-2-SA (without AgNPs, red full symbols). Indeed, Fig. A6 shows that the Ps fraction $F_{3\gamma}$ is similar for samples PHEMA-SA-Ag and PHEMA-DEG-2-SA. These results strongly indicate that in presence of crosslinker the brushes display a closer structure and, as a result, smaller AgNPs are formed (33 ± 14 nm without crosslinker, 23 ± 8 nm and 12 ± 5 nm with 2% and 4% of crosslinker). Consequently, increased *ortho*-Ps formation is observed which leads to an increased *S*-parameter. A similar behavior was recently observed by us in poly(dimethylaminoethyl methacrylate) brushes after loading pre-synthesized AgNPs [15].

To estimate the densities of the different brush layers and the volume fractions of silver inside the brushes, a VEPFIT model was used [28]. The VEPFIT software is a best-fit procedure based on the solution of the diffusion equation for positrons in each layer of a heterostructure, taking into account the energy dependent positron implantation profiles. The model free parameters, for each layer, are the following: the *S*-parameter value, the positron diffusion length, the thickness and the layer density. The density and the thickness are correlated parameters and it is only possible to obtain an estimation of one of these if the other is known. Thickness values were measured by means of ellipsometry, as mentioned before: 130 ± 7 nm for sample PHEMA-SA, 115 ± 12 nm for PHEMA-DEG-2-SA and 167 ± 10 nm for PHEMA-DEG-4-SA. Thus, the mass density was estimated by minimizing the variance of the fit.

The *S*-parameter data presented in Fig. 4 were fitted with VEPFIT to estimate the layer densities.

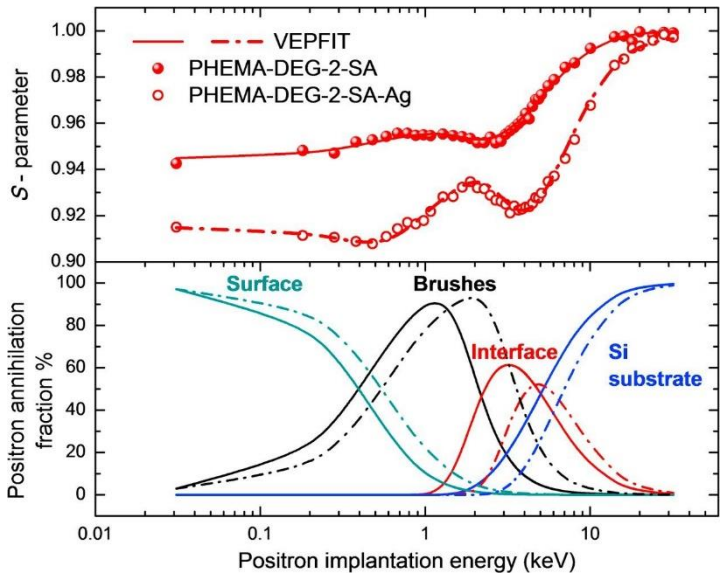

Fig. 4. *S*-parameter and positron annihilation fraction as a function of the positron implantation energy for the brush-gel prepared with 2 mol% of crosslinker, with and without AgNPs. The continuous and dashed lines correspond to samples without and with Ag, respectively.

To fit the experimental data, at first a model comprising three layers (substrate, brush and brush surface i.e. the brush/vacuum interface) was chosen. However, PAS data showed the presence, in the 3–6 keV energy range for the AgNPs-loaded samples and 2–4 keV for the other samples, of an additional layer which could be interpreted - and included in the fitting model - as an interface between the brush and the silicon substrate. This interface is about 2–4 nm thick, it is formed by the ATRP initiator molecules and the silicon

oxide layer that passivates the silicon surface. For this reason, a four layers-model was chosen comprising a surface, a brush layer, a brush/substrate interface and the silicon substrate. The upper frames of Fig. 4 contain only the experimental data of samples PHEMA-DEG-2-SA and PHEMA-DEG-2-SA-Ag (the results obtained for the other samples are shown in Fig. A8). The continuous and dashed lines through data points of Fig. 4 represent the best fits. The fractions of positrons that annihilate inside each layer after implantation and diffusion are depicted in the lower frame of this figure. The value of the *S*-parameter can be considered as a linear combination given by:

$$S(E) = \sum_{i}^{layer} f_i(E) S_i \tag{5}$$

where S_i and $f_i(E)$ are the *S*-parameter and fraction of positrons that annihilate in each layer at a given implantation energy. The *S*-parameter of the S_i substrate was normalized and fixed to one. After several tests with free parameters it was observed that the value of the *S*-parameter of the interface tends to 0.943 and 0.890 (with an error of 0.001 in both cases) for all samples, respectively before and after the formation of AgNPs. As mentioned before, it was observed an effect of Ps inhibition after NPs formation that justifies this finding. The *S*-parameter values of the surface and the brushes as obtained from the fit are shown in Table 1, Table 2.

Table 1. *S*-parameter and mass density obtained by means of VEPFIT for the brushes prepared with different crosslinker amounts (0, 2 and 4 mol%).

Sample	*S*-parameter Surface	Brushes	ρ_B [g cm^{-3}]	χ^2/DoF
PHEMA-SA	0.932 ± 0.001	0.950 ± 0.001	0.95 ± 0.15	1.24
PHEMA-DEG-2-SA	0.942 ± 0.001	0.957 ± 0.001	1.19 ± 0.15	1.48
PHEMA-DEG-4-SA	0.930 ± 0.001	0.950 ± 0.001	1.23 ± 0.15	1.29

Table 2. *S*-parameter, mass density and volume fraction of AgNPs obtained by means of VEPFIT for brushes loaded with NPs prepared with different crosslinker amounts (0, 2 and 4 mol%).

Sample	*S*-parameter Surface	Brushes	ρ_B [g cm^{-3}]	vf	n × 10^{16} [cm^{-3}]	χ^2/DoF
PHEMA-SA-Ag	0.940 ± 0.001	0.950 ± 0.001	2.75 ± 0.25	0.19 ± 0.04	1.0 ± 0.5	1.47
PHEMA-DEG-2-SA-Ag	0.913 ± 0.001	0.943 ± 0.001	2.73 ± 0.25	0.17 ± 0.04	2.7 ± 1.1	1.22
PHEMA-DEG-4-SA-Ag	0.912 ± 0.001	0.929 ± 0.001	2.40 ± 0.25	0.13 ± 0.05	14 ± 8	1.65

The mass density of the polymer layers with and without Ag were estimated by minimizing the variance of the fits i.e. the chi-square divided the degrees of freedom χ^2/DoF (see Fig. A9) [15], [29]. The average molecular mass M_n values for the polymer chains were calculated using the obtained density values (see Appendix A). The density of the brushes without AgNPs is in good agreement with the value reported for bulk PHEMA (1.15 g mL^{-1}). The density values show an obvious increase, between 10% and 20% over the whole brushes, in presence of silver nanoparticles (the density of bulk Ag being 10.49 g cm^{-3}). Eventually, the volume fraction v_f of AgNPs inside the brushes was estimated according to the following relationship:

$$\rho = \rho_{Ag}\, v_f + \rho_{Brushes}\,(1 - v_f) \tag{5}$$

where ρ is the density of the brushes loaded with silver, $\rho_{Ag}\, v_f$ is the bulk Ag density and $\rho_{Brushes}$ is the brushes density estimated for the sample without AgNPs and the same amount of crosslinker. The v_f values (Table 2) are 10–20% within the experimental error. The number density *n*, defined as the ratio of the volume fraction v_f to the average volume of the AgNP (under the hypothesis of sphericity), increases from about 10^{16} to 10^{17} cm^{-3} as a function of crosslinking. The distribution and dimension of the AgNPs clearly depends on the content of crosslinker and the finest distribution of AgNPs was observed for the brush-gels obtained with the higher crosslinker contents (4 mol% of DEGDMA).

4. Conclusions

Positron Annihilation Spectroscopy (PAS) proved to be a powerful resource for the study of polymer brushes. The ability of PAS to help discriminating between brush-gels obtained with different amounts of DEGDMA crosslinker was demonstrated, as well as its suitability to give information about conformational changes experienced by brushes and brush-gels after loading with silver nanoparticles, allowing to calculate the distribution and mass concentration of the latter inside the brushes. Noteworthy, all these results were obtained by one single analysis and without making the least damage to the samples. Given such advantages, Position Annihilation Spectroscopy will soon impose as a key technique to unlock many of the mysteries of polymer brushes and brush-gels.

Acknowledgements

The authors thank Moh Divandari, Edmondo M. Benetti, Antonella Rossi and Giovanni Cossu (ETH Zürich) for their valuable advice and discussions. Parts of this research were carried out at the Helmholtz-Zentrum Dresden-Rossendorf e. V., a member of the Helmholtz Association.

References

[1] S.T. Milner, Polymer Brushes, Science (80-.), 251 (1991), pp. 905-914, http://dx.doi.org/10.1017/CBO9781107415324.004
[2] G. Panzarasa, The art and science of polymer brushes: Recent developments in patterning and characterization approaches, Chimia (Aarau)., 71 (2017), http://dx.doi.org/10.2533/chimia.2017.354
[3] F. Zhou, W.T.S. Huck, Surface grafted polymer brushes as ideal building blocks for “smart” surfaces, Phys. Chem. Chem. Phys., 8 (2006), pp. 3815-3823, http://dx.doi.org/10.1039/b606415a
[4] L. Ionov, N. Houbenov, a. Sidorenko, M. Stamm, S. Minko, Smart Microfluidic Channels, Adv. Funct. Mater, 16 (2006), pp. 1153-1160, http://dx.doi.org/10.1002/adfm.200500562
[5] J. Klein, E. Kumacheva, D. Mahaiu, D. Perahia, L.J. Fetters, Reduction of frictional forces between solid surfaces bearing polymer brushes, Nature (ISSN 0028-0836)., 370 (1994), pp. 634-636, http://dx.doi.org/10.1038/370634a0
[6] S.J. Lue, J.J. Hsu, T.C. Wei, Drug permeation modeling through the thermo-sensitive membranes of poly(N-isopropylacrylamide) brushes grafted onto micro-porous films, J. Memb. Sci., 321 (2008), pp. 146-154, http://dx.doi.org/10.1016/j.memsci.2008.04.053
[7] A. Kusumo, L. Bombalski, Q. Lin, K. Matyjaszewski, J.W. Schneider, R.D. Tilton, High capacity, charge-selective protein uptake by polyelectrolyte brushes, Langmuir, 23 (2007), pp. 4448-4454, http://dx.doi.org/10.1021/la063660b
[8] K. Wolski, M. Szuwarzyński, S. Zapotoczny, A facile route to electronically conductive polyelectrolyte brushes as platforms of molecular wires, Chem. Sci., 6 (2015), pp. 1754-1760, http://dx.doi.org/10.1039/C4SC04048A
[9] D.M. Loveless, N.I. Abu-Lail, M. Kaholek, S. Zauscher, S.L. Craig, Reversibly cross-linked surface-grafted polymer brushes, Angew. Chemie - Int. Ed., 45 (2006), pp. 7812-7814, http://dx.doi.org/10.1002/anie.200602508
[10] E.S. Dehghani, V.V. Naik, J. Mandal, N.D. Spencer, E.M. Benetti, Physical networks of metal-ion-containing polymer brushes show fully tunable swelling and nanomechanical and nanotribological properties, Macromolecules (2017), http://dx.doi.org/10.1021/acs.macromol.6b02673
[11] E.S. Dehghani, N.D. Spencer, S.N. Ramakrishna, E.M. Benetti, Crosslinking polymer brushes with ethylene glycol-containing segments: Influence on physicochemical and antifouling properties, Langmuir, 32 (2016), pp. 10317-10327, http://dx.doi.org/10.1021/acs.langmuir.6b02958

[12] F. Costantini, E.M. Benetti, R.M. Tiggelaar, H.J.G.E. Gardeniers, D.N. Reinhoudt, J. Huskens, et al., A brush-gel/metal-nanoparticle hybrid film as an efficient supported catalyst in glass microreactors, Chem. - A Eur. J., 16 (2010), pp. 12406-12411, http://dx.doi.org/10.1002/chem.201000948
[13] E.M. Benetti, X. Sui, S. Zapotoczny, G. Julius, Vancso, Surface-grafted gel-brush/metal nanoparticle hybrids, Adv. Funct. Mater., 20 (2010), pp. 939-944, http://dx.doi.org/10.1002/adfm.200902114
[14] S. Christau, J. Genzer, R. von Klitzing, Polymer Brush/Metal Nanoparticle Hybrids for Optical Sensor Applications: from Self-Assembly to Tailored Functions and Nanoengineering, Zeitschrift Für Phys. Chemie., 229 (2014), pp. 1089-1117, http://dx.doi.org/10.1515/zpch-2014-0573
[15] G. Panzarasa, S. Aghion, G. Soliveri, G. Consolati, R. Ferragut, Positron annihilation spectroscopy: a new frontier for understanding nanoparticle- loaded polymer brushes, Nanotechnology, 27 (2016), p. 02LT03, http://dx.doi.org/10.1088/0957-4484/27/2/02LT03
[16] G. Panzarasa, S. Aghion, G. Marra, A. Wagner, M.O. Liedke, M. Elsayed, et al., Probing the impact of the initiator layer on grafted-from polymer brushes: a positron annihilation spectroscopy study, Macromolecules., 50 (2017), pp. 5574-5581, http://dx.doi.org/10.1021/acs.macromol.7b00953
[17] W. Huang, J.B. Kim, M.L. Bruening, G.L. Baker, Functionalization of surfaces by water-accelerated atom-transfer radical polymerization of hydroxyethyl methacrylate and subsequent derivatization. Macromolecules, 35 (2002), pp. 1175-1179, http://dx.doi.org/10.1021/ma011159e
[18] S. Sanjuan, P. Perrin, N. Pantoustier, Y. Tran, Synthesis and Swelling Behavior of pH-Responsive Polybase Brushes, Langmuir., 23 (2007), pp. 5769-5778, http://dx.doi.org/10.1021/la063450z
[19] W. Anwand, G. Brauer, M. Butterling, H.R. Kissener, A. Wagner, Design and construction of a slow positron beam for solid and surface investigations, Defect Diffus. Forum., 331 (2012), pp. 25-40, http://dx.doi.org/10.4028/www.scientific.net/DDF.331.25
[20] G. Consolati, R. Ferragut, A. Galarneau, F. Di Renzo, F. Quasso, Mesoporous materials for antihydrogen production, Chem. Soc. Rev., 42 (2013), pp. 3821-3832, http://dx.doi.org/10.1039/c2cs35454c
[21] D.G. Castner, Characterization of Poly(2-Hydroxyethyl Methacrylate) (PHEMA) by XPS, Surf. Sci. Spectra., 4 (1996), p. 14, http://dx.doi.org/10.1116/1.1247807
[22] E.S. Dehghani, S.N. Ramakrishna, N.D. Spencer, E.M. Benetti, Controlled crosslinking is a tool to precisely modulate the nanomechanical and nanotribological properties of polymer brushes, Macromolecules., 50 (2017), pp. 2932-2941, http://dx.doi.org/10.1021/acs.macromol.6b02409
[23] E.M. Benetti, J.C. Hong, G.J. Vancso, pH responsive polymeric brush nanostructures: Preparation and characterization by scanning probe oxidation and surface initiated polymerization, Macromol. Rapid Commun., 30 (2009), pp. 411-417, http://dx.doi.org/10.1002/marc.200800628
[24] G.W. Rubloff, Defect microchemistry in SiO2/Si structures, J. Vac. Sci. Technol. A, 8 (1990), pp. 1857-1863
[25] K.G. Lynn, D.O. Welch, Slow positrons in metal single crystals. I. Positronium formation at Ag(100), Ag(111), and Cu(111) surfaces, Phys. Rev. B., 22 (1980), pp. 99-110, http://dx.doi.org/10.1103/PhysRevB.22.99
[26] E. Soininen, H. Huomo, P.a. Huttunen, J. Mäkinen, a. Vehanen, P. Hautojärvi, Temperature dependence of positron diffusion in cubic metals, Phys. Rev. B., 41 (1990), pp. 6227-6233, http://dx.doi.org/10.1103/PhysRevB.41.6227
[27] S. Aina, A. Dupasquier, V. Thakur, S.B. Shrivastava, M.K. Rathore, T. Leguey, et al., Positron annihilation studies of the multilayer Cu – Cu 3 Sn system, J. Phys. Condens. Matter., 10 (1998), pp. 10827-10838
[28] A. Van Veen, H. Schut, J. De Vries, R.A. Hakvoort, M.R. Ijpma, Analysis of positron profiling data by means of "'VEPFIT'", AIP Conf. Proc., 218 (1991), pp. 171-198, http://dx.doi.org/10.1063/1.40182
[29] X. Yu, J. Smith, N. Zhou, L. Zeng, P. Guo, Y. Xia, et al., Spray-combustion synthesis: efficient solution route to high-performance oxide transistors, Proc. Natl. Acad. Sci. USA, 112 (2015), pp. 3217-3222, http://dx.doi.org/10.1073/pnas.1501548112

Appendix A

Table A1: Relative areas (as %) from the component peaks of C 1s peaks from XPS for the different polymer films.

	(C-C) %	(O-C-C-O) %	(C=O) %	(q-C) %	(C-OH) %
PHEMA	33.6	17.2	16.4	16.1	16.8
PHEMA-DEG2	32	19.4	15.9	17.5	15
PHEMA-DEG4	30.2	22.0	15.1	19.2	13.4

Table A2: Angle-resolved XPS data obtained for the C 1s peak to Ag 3d peak ratio at different emission angles for different brush systems. The signal of C/Ag decreased from the surface (26.7° emission angle), to the bulk (79.2° emission angle), thus the presence of Ag is not limited only to the outer most surface of the films and is seen throughout the lateral profile.

Emission angle (°)	PHEMA-SA (%)	PHEMA-DEG2-SA (%)	PHEMA-DEG4-SA (%)
26.7	63 ± 1	80 ± 2	73 ± 1
34.2	64 ± 1	81 ± 2	72 ± 1
41.7	63 ± 3	80 ± 1	72 ± 1
49.2	63 ± 2	79 ± 1	70 ± 1
56.7	60 ± 1	78 ± 1	68 ± 1
64.2	59 ± 2	77 ± 1	66 ± 1
71.7	56 ± 2	74 ± 1	62 ± 1
79.2	53 ± 2	71 ± 1	59 ± 1

ESTIMATION OF THE AVERAGE MOLAR MASS M_n

The average molar mass M_n of the grafted polymer chains could be estimated using the well-known relationship (eq. A1)[1] between the surface density of chains σ (assumed to be 0.5 chains nm^{-2}), the thickness h of the polymer layer (measured by ellipsometry), the density ρ of the polymer layer (extracted from PAS data) and Avogadro's number N_A:

$$M_n = {}^{N_A h \rho}/_{\sigma} \qquad \text{(A1)}$$

The results are summarized in Table A3.

Table A3: Estimated M_n values for the investigated polymer brushes.

Sample name	*Estimated average* M_n (g mol^{-1})
PHEMA-SA	$1.5 \cdot 10^5$
PHEMA-DEG2-SA	$1.6 \cdot 10^5$
PHEMA-DEG4-SA	$2.5 \cdot 10^5$

[1] D. M. Jones, A. Brown, W. T. S. Huck. *Langmuir* 13 (2002) 1265−1269.

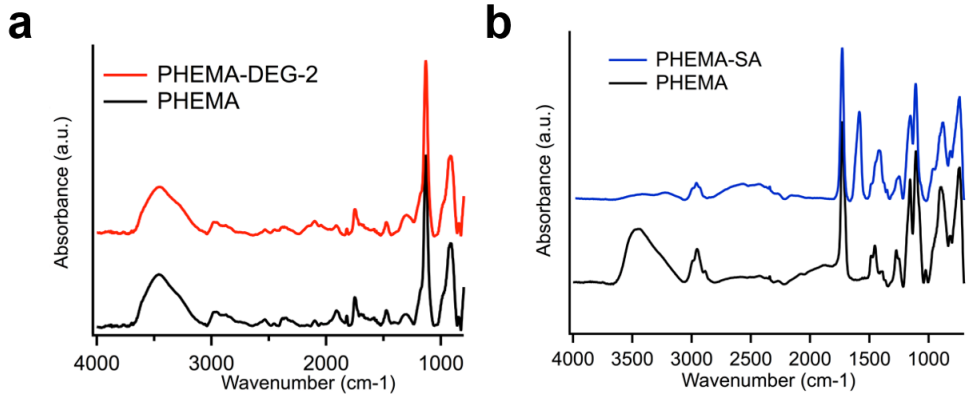

Figure A1. Representative FT-IR spectra of a) PHEMA brushes and PHEMA brushes synthesized with 2% of crosslinker (PHEMA-DEG-2) brush-hydrogel; b) PHEMA brushes and succinic anhydride-modified PHEMA brushes (PHEMA-SA).

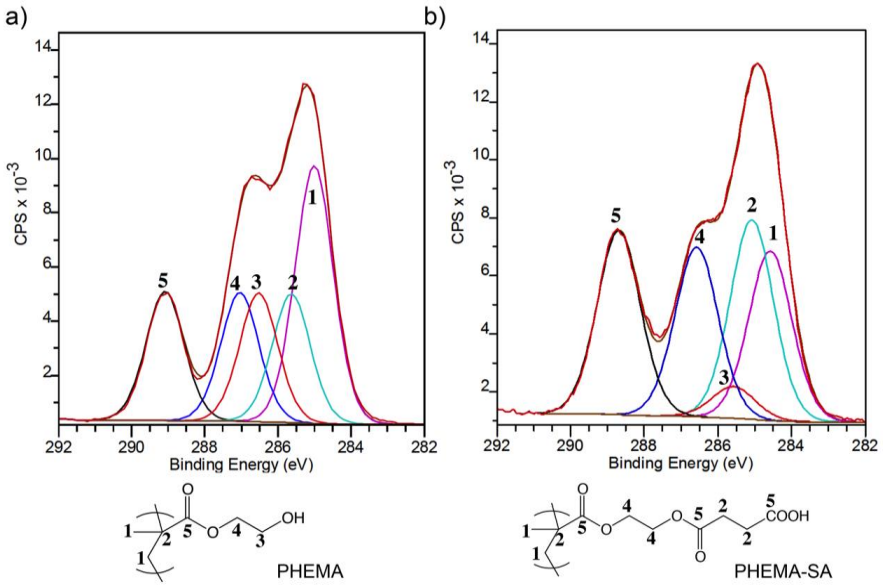

Figure A2. C1s XPS spectrum recorded on PHEMA brushes and the corresponding curve-fit using five spectral components (a); C1s XPS spectrum for PHEMA-SA brushes with the corresponding curve-fit obtained by applying five spectral components structure (b). The unreacted C-OH group is highlighted as peak 3.

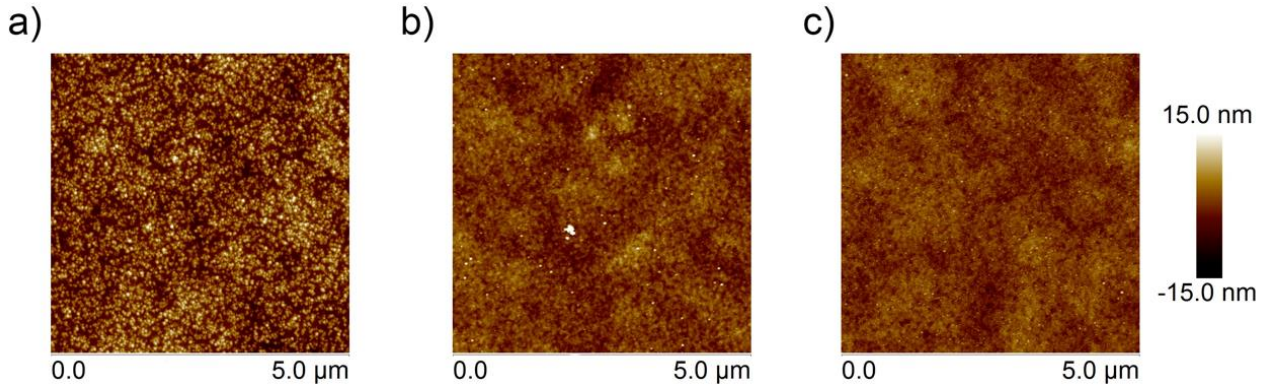

Figure A3. AFM images (tapping mode) of brushes and brush-gels: a) PHEMA-SA; b) PHEMA-DEG2-SA; c) PHEMA-DEG4-SA. The samples were analyzed in the dry state.

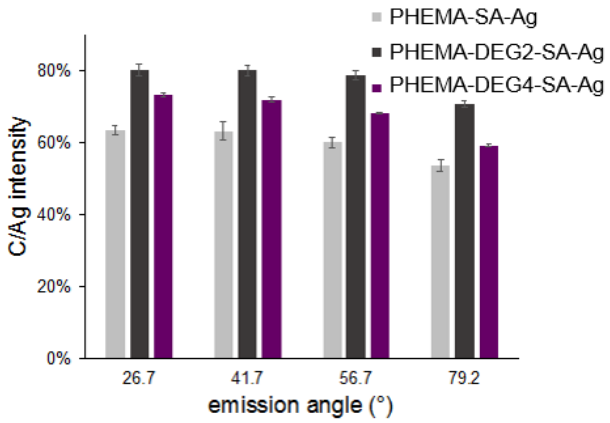

Figure A4. C 1s peak to Ag 3d peak ratio at different emission angles for brushes and brush-gels loaded with silver nanoparticles. The C/Ag value at the lowest angle (26.7°) represents bulk-sensitive measurements, while the C/Ag value at the highest angle (79.2°) provides information about the samples' surface.

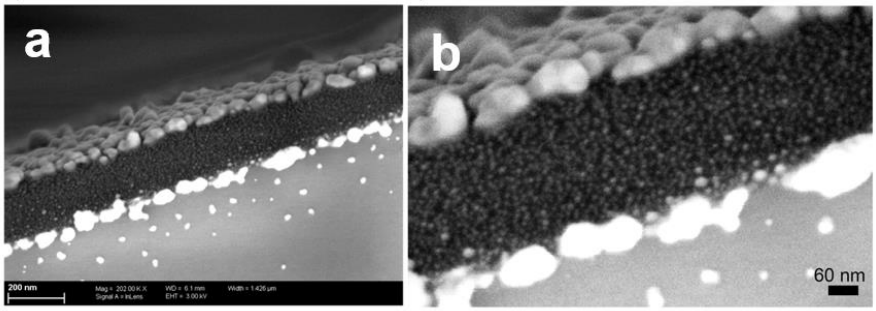

Figure A5. (a) and (b): Scanning electron microscopy (SEM) image of the cross-section of sample PHEMA-SA-Ag, where silver nanoparticles, which formed within the polymer chains (bright dots), are homogeneously dispersed in the polymer layer.

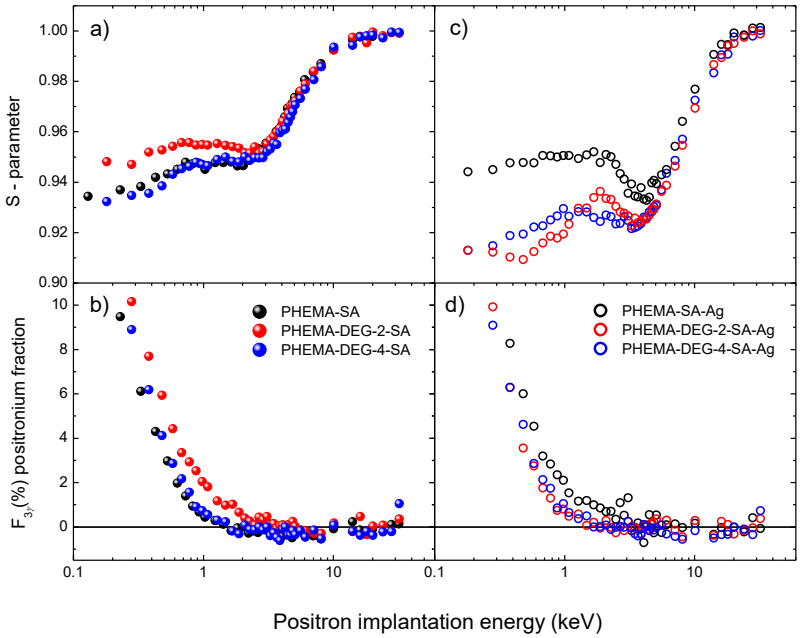

Figure A6. *S*-parameter and Ps fraction $F_{3\gamma}$ as a function of the positron implantation energy. The probability α to annihilate into the AgNPs depends on the ratio of NPs diameter d and the positron diffusion length in silver L_+ following the Langevin function[2]:

$$\alpha = \coth\left(d/L_+\right) - L_+/d \qquad \text{(A2)}$$

[2] J. Dryzek, A. Czapla, E. Kusior. *J. Phys.: Condens. Matter* **10** (1998) 10827.

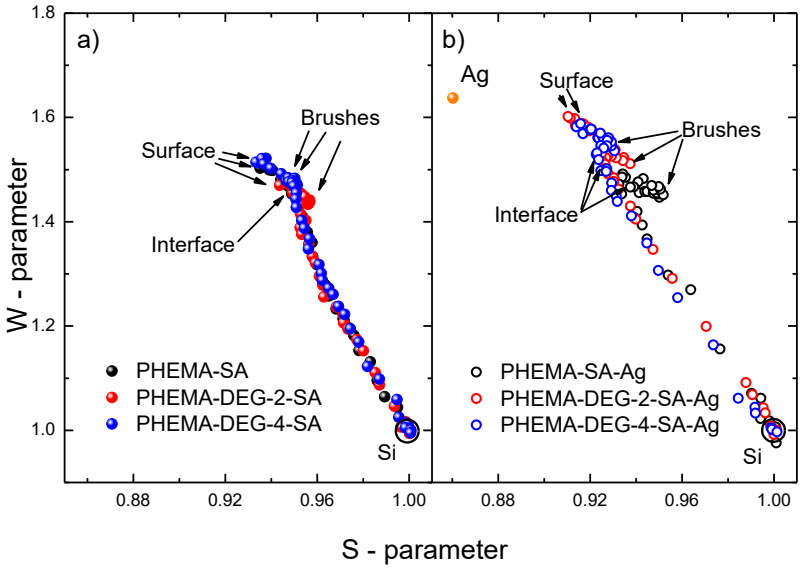

Figure A7. *W*-parameter as a function of the *S*-parameter (refer to Figure 4 in the manuscript).

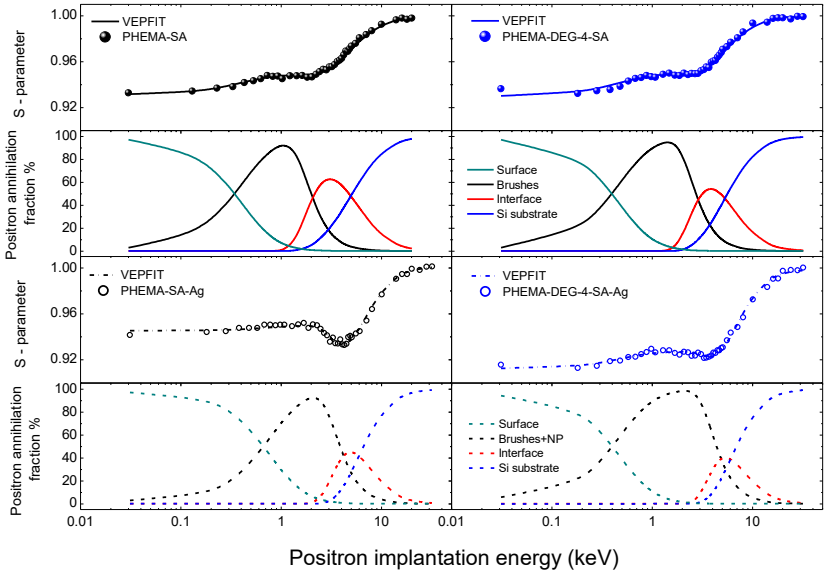

Figure A8. *S*-parameter and positron annihilation fraction as a function of the implantation energy in samples with and without AgNPs and with 0 and 4% of crosslinker. The continuous and dashed lines correspond to samples without and with Ag, respectively.

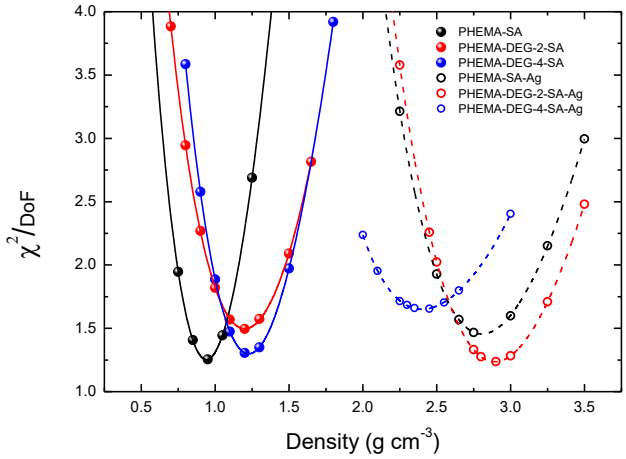

Figure A9. Variance of the fit (Chi-square divided the degrees of freedom) of the *S*-parameter (calculated for thicknesses values obtain by means of ellipsometry) as a function of the number density of the brush films.